Korean J. Chem. Eng., 39(6), 1588-1596 (2022)
DOI: 10.1007/s11814-022-1089-0

pISSN: 0256-1115
eISSN: 1975-7220

Desalination and lignin concentration in a lignin aqueous solution by nano-filtration process: Advanced γ-Al_2O_3 film-coated porous α-Al_2O_3 hollow fiber membrane

Xuelong Zhuang*, Min Chang Shin*, Byeong Jun Jeong*, Jae Yeon Hwang*, Young Chan Choi, and Jung Hoon Park*,†**

*Department of Chemical and Biochemical Engineering, Dongguk University, 30, Pildong-ro 1 gil, Jung-gu, Seoul 04620, Korea
**Fine Dust Research, Korea Institute of Energy Research (KIER), Daejeon 34129, Korea
(*Received 24 August 2021 • Revised 14 February 2022 • Accepted 20 February 2022*)

Abstract−To remove the main barrier for lignin valorization, which is the development of actual lignin separation technology, we studied the ceramic membrane nanofiltration process using a dense, ultra-thin γ-Al_2O_3 film-coated porous α-Al_2O_3 hollow fiber ($\gamma\,\alpha$ HF) membrane for the simultaneous separation of alkali metals (Na^+, K^+, etc) and concentration of lignin from an alkaline media like black liquor with success as an advanced wastewater treatment process. The γ-AlOOH sol was prepared by sol-gel method and coated by dip-coating on α-Al_2O_3 hollow fiber (α HF) support. After calcination at high temperature, the mean pore sizes of the α HF support and the $\gamma\,\alpha$ HF membrane were found to be 0.2 μm and 1.6 nm. The rejection rate performance for various salts increased in the following order: Na_2SO_4<$MgSO_4$<NaCl<KCl<$CaCl_2$<$MgCl_2$<$AlCl_3$. Under the best condition, the removal rate of sodium and potassium ions reached about 92% and 85%, respectively, with 19.34% of the lignin being discharged. The $\gamma\,\alpha$ HF membrane presents good performance stability during a five day nano-filtration process.

Keywords: Lignin Valorization, Ion Removal Process, Hollow Fiber Membrane, Nanofiltration Membrane, Wastewater Resources

INTRODUCTION

From an environmental viwepoint, lignocellulose (35-50% cellulose, 20-35% hemicellulose, and 14-26% lignin) is the most abundant complex of natural polymers on Earth, and it represents about one-third of the total organic carbon in the biosphere and one-third of wood [1]. Lignin is a complex three-dimensional macromolecule consisting of phenyl propane units. During the production of common white paper, the lignin must be separated from cellulose because its presence in the final mixture gives a light brown appearance [1]. During this process, lignin organic wastes from papermaking industries, which are a complex mixture of organic and inorganic molecules in nature, are generated annually in the world, and this amount is expected to rise soon [2,3]. Advancement in waste valorization technologies to improve separation and then utilization of lignin as a potential source of aromatic polymers and green energy is an essential aspect of bio-economy and future biorefineries [2,4]. Ahmad provides a comprehensive overview of potential products that can be obtained from the lignin conversion and their potential market [5].

The most utilized process to obtain lignin from the lignocellulose is called the Kraft process. The core of the chemical pulping process is a cooking step where the lignocellulosic biomass in the form of chips is placed in a digester at about 150-180 °C along with cooking chemicals, including water, sodium hydroxide (NaOH), and sodium sulfide (Na_2S), to promote the dissociation of the cellulose fibers. The obtained fiber suspension called "brown stock" is subsequently washed to separate an unbleached pulp of cellulosic fibers from an alkaline organic aqueous solution, named weak black liquor, mainly composed of a mixture of NaOH, Na_2S, lignin, and other organic polymers [5]. Consequently, from the perspective of the conversion of lignin into value-added chemicals, the further development of lignin separation technology remains a challenging task [1-6].

In recent years, there has been wide interest in developing advanced nanofiltration membranes for water and wastewater treatment and desalination [7-9]. Most experimental studies on nanofiltration membranes for lignin separation are conducted with polymeric membranes due to their good film-forming property and suitable flexibility [7,10] but, in general, very few polymeric membranes have been reported in the literature that can be used in an acid or alkaline aqueous environment [11,12]. In most previous studies polymeric membranes have been studied [7-10,13-20]. However, the polymeric membrane has some intrinsic limitations, especially with high black liquor temperature and high black liquor PH [21]. Although there are a great number of studies for the development of polymeric nanofiltration membranes [10,13-20], the inorganic nanofiltration membranes with superior separation performance and chemical/physical stability properties are needed for the conversion of lignin into value-added chemicals in acidic and alkaline media like black liquor [22-31] in a flat configuration [10, 13-16,18,19] and a tubular form [20,22-25,27-31]. In detail, the tubular membranes used throughout all recent literature were commercial ceramic membranes like KERASEP membrane coated with ZrO_2 manufactured by Orelis [22-24], alumina coated with an inner

†To whom correspondence should be addressed.
E-mail: pjhoon@dongguk.edu

skin layer of either TiO_2 or ZrO_2 (CrRAM INSIDE 25 ®) fabricated by TAMI Industries [25], Al_2O_3-TiO_2 membrane with an active layer of ZrO_2 [26], ultrasil 10 (0.5 wt%) [27], ceramic membrane marketed by IBMEM – Industrial Biotech Membranes (Frankfurt, Germany) [28], Al_2O_3 membrane with a surface layer of TiO_2 [29], TiO_2 membrane [30], and ZrO_2 membrane produced by Altech Germany [31],

Since the 1990s many researchers have proposed new pure inorganic nanofiltration membranes to further study promising inorganic alternatives with a pore size smaller than 1-2 nm [32]. Puhlfürß et al. developed a microporous TiO_2 membrane by a polymeric sol-gel technique on top of a specially designed tubular ceramic multi-layer support [33]. Van Gestel et al. studied the disk-shaped and tubular ceramic nanofiltration membranes with a multilayer configuration: α-Al_2O_3 macroporous support, a membrane interlayer of Al_2O_3, TiO_2, and mixed Al_2O_3-TiO_2. and an active very thin TiO_2 top layer [34]. Supported γ-Al_2O_3 nanofiltration membrane where the support consisted of an Al_2O_3 disk-shaped has proven to be very effective for the removal of an oily hydrocarbon contaminant from wastewater [35]. Qi et al. manufactured a disk α-Al_2O_3 microfiltration membrane as supported by colloidal filtration route and deposited titania supported γ-Al_2O_3 mesoporous layer on the surface by dip-coating method [36].

Therefore, much research to date has focused on ceramic nanofiltration membranes with disk [34-36] and tubular shapes [33,37]. However, very little work has been done on the Al_2O_3 hollow fiber ceramic membrane for nanofiltration applications [37]. In detail, Wang et al. studied asymmetric multilayer membranes based on a porous α-Al_2O_3 hollow fiber support layer with TiO_2 and γ-Al_2O_3 as intermediate and top layers, respectively, and they obtained an γ-Al_2O_3/α-Al_2O_3 hollow fiber ceramic membrane for nanofiltration process [37].

This work studied and evaluated a novel inorganic membrane nanofiltration process for the simultaneous separation of alkali metals (Na^+, K^+, etc) and concentration of lignin from an alkaline media like black liquor. The original idea behind this work is to further study the dense, ultra-thin γ-Al_2O_3 film-coated porous α-Al_2O_3 hollow fiber membrane and apply it for purification and concentration of lignin in alkaline media.

To the best of our knowledge, this is one of the first studies that consider a one-step nano-filtration process for lignin desalination and concentration from an alkaline lignin aqueous solution through an advanced dense, ultra-thin γ-Al_2O_3 film-coated porous α-Al_2O_3 hollow fiber ($\gamma\,\alpha$ HF) membrane.

EXPERIMENTAL

1. Materials

α-Al_2O_3 powder (<0.5 μm) and Polyethersulfone (PESf) were purchased from Kceracell (Korea) and Ultrason® (DEU), respectively. Polyvinylpyrrolidone (PVP, 99.5%) and polyvinyl alcohol (PVA, MW=1,800 Da) both were acquired from Sigma-Aldrich (USA). Sodium sulfate (Na_2SO_4, 99.0%), magnesium sulfate ($MgSO_4$, 98.0%), sodium chloride (NaCl, 99.0%), potassium chloride (KCl, 99.0%), magnesium chloride ($MgCl_2$, 99.0%), calcium chloride ($CaCl_2$, 99.0%) and aluminum chloride ($AlCl_3$, 99.0%), and 1-Methyl-2-pyrrolidinone anhydrous (NMP, 99.5%), Aluminum isopropoxide (AIP, 98%), Nitric acid (HNO_3, 60%) and Polyethylene glycol (PEG) - with 200 Da, 400 Da, 600 Da, 800 Da, 1,000 Da, 1,500 Da, 2,000 Da, 4,000 Da, 6,000 Da molecular weight - were acquired from Samchun Pure Chemical Co Ltd (Korea). All reagents were used as received without further purification.

2. Preparation of α-Al_2O_3 Hollow Fiber (α HF) Support

Based on our previous experience in the synthesis of α-Al_2O_3 hollow fiber membrane by a phase inversion process [38,39], porous α HF support was successfully obtained by using a similar experimental procedure and conditions, except that the particle size of the α-Al_2O_3 precursor was increased. In a typical procedure, a first solution was obtained by adding 36 g PESf to 201 g NMP followed by stirring at 150 rpm for 24 hours at room temperature. After this process, 3 g PVP and 360 g α-Al_2O_3 powder were added to the first solution and then stirred again at 300 rpm for 24 hours. The prepared casting solution was placed in a stainless reactor in a vacuum of 0.8 bar for 1 hour for degassing purposes. The nitrogen pressure used was 3 Mpa and the air gap distance was fixed at 10 cm with a water flow of 10 ml/min. After the spinning procedure, the prepared green body was put in water for 24 hours to remove residual organic solvents and then dried overnight in a static oven at 90 °C to remove surface and internal moisture. Finally, the α HF support was sintered in a furnace at 1,300 °C (heating speed=3 °C/min) and kept at the temperature for three hours in static air.

3. Preparation of γ-Al_2O_3 Coating Solution

In the first step of the preparation, 0.05 mol AIP was added to 90 ml hot water at 60 °C and then stirred for 1 hour at 600 rpm in an oil bath at 82 °C to completely hydrolyze aluminum isopropoxide. The second step consisted of adding 0.0125 mol HNO_3 to the AIP aqueous solution and heating the mixture at 90 °C. The obtained precursor was stirred for 2 hours in a closed container to form a sol of aluminum oxide particles. With the aim of evaporating the isopropanol generated during the hydrolysis reaction, the obtained colloid was placed in an open container at 90 °C for 1.5 hours. Finally, the sol was aged at 90 °C for 15 hours using a condensation reflux device. Finally, a γ-AlOOH sol completely transparent was obtained. Before the single dip-coating deposition of γ-AlOOH sol on the surface of α HF support, 5 wt% PVA was used as a drying chemical control additive.

4. Preparation of γ-Al_2O_3 Film-coated Porous α-Al_2O_3 Hollow Fiber ($\gamma\,\alpha$ HF) Membrane

The $\gamma\,\alpha$ HF membranes were prepared by a single dip-coating process. In detail, the γ-AlOOH sol was coated on the shell side of α HF support by dip-coating method to obtain the $\gamma\,\alpha$ HF membrane. Before the dip-coating process, the α HF support was sonicated in distilled water for 1 hour. The immersion and pulling speeds were both set to 1 mm/s. The immersion time was set to 120 seconds. The whole dip-coating process had to be carried out under 30% RH. The obtained membrane was dried at room temperature for 24 hours and then was calcinated into a static furnace at 350 °C (heating rate=1 °C/min) for 2 hours to obtain the $\gamma\,\alpha$ HF membrane.

5. Characterization of α HF Support and $\gamma\,\alpha$ HF Membrane

The pore sizes of α HF support and $\gamma\,\alpha$ HF membrane were measured by the gas permeability method under different nitrogen

pressures at a specific temperature. The slope (S_0) and the intersection (I_0) of the linear regression obtained in the permeability-permeation pressure graph were used to evaluate the average pore size of the sample. The average pore size (d_h) is calculated as follows [40,41]:

$$d_h = \frac{32}{3}\frac{S_0}{I_0}\left(\frac{8RT}{\pi M_n}\right)^{0.5}\mu \quad (1)$$

where R is the nitrogen gas constant, and T is the temperature. The M_n is the molecular weight of nitrogen, and μ is the gas viscosity of nitrogen.

Scanning electron microscope analysis (SEM, NovaNano SEM450/FEI, USA) was used to characterize the prepared α HF support and $\gamma\,\alpha$ HF membrane. The water contact angle was determined by the contact angle measurement (Seo Phoenix-I, Korea). The membrane porosity ε (%) was measured using the gravimetric method [42]. In particular, the sample was immersed in distilled water for 48 hours and then the water in the lumen side was blown out with a flux of nitrogen gas. The water on the surface was wiped off, and the weight (m_{wet}) was measured. In a second step, the sample was put into an oven at 105 °C for 48 hours so that the weight (dry) was recorded. The following formula was used to calculate the porosity:

$$\varepsilon = \frac{\Delta m}{V\rho_{H_2O}} \times 100\% = \frac{m_{wet} - m_{drt}}{\frac{\pi}{4}(d_0^2 - d_i^2)l\rho_{H_2O}} \times 100\% \quad (2)$$

where d_0 and d_i are the outer (cm) and inner diameter (cm) of the membrane. l and ρ_{H_2O} are the length (cm) of the membrane and water density (1.0 g cm^{-3}) at room temperature.

A zeta potential analysis was also carried out to study the change of surface in different preparation conditions. A part of the γ-AlOOH sol was dried at 60 °C and then calcined into a static furnace at 350 °C (heating rate=1 °C/min) for 2 h. The γ-Al_2O_3 powders were partitioned in distilled water and the pH of the colloidal suspension was adjusted with HCl and NaOH. Zeta potential analysis was carried out using a Zeta-Potential & Particle Size Analyzer (ELSZ-2000Z, Otsuka Electronics Co., Ltd. JAPAN).

6. Membrane Permeation Test

The module was made of five $\gamma\,\alpha$ HF membranes with an effective membrane area of 53 cm^2. The feed was pumped into the shell side of the $\gamma\,\alpha$ HF membrane with a constant flow rate of 280 ml/min. To ensure the stable state of the membrane during the experiment, distilled water was pre-compressed at 5 bar until the permeate was stable. All permeation tests were at room temperature and under a pressure of 5 bar unless otherwise specified. The results of the permeation tests were recorded until the flux of permeation reached equilibrium values.

The feed for permeation test was pure distilled water and aqueous solution with different solutes, such as NaCl, KCl, $CaCl_2$, $MgCl_2$, Na_2SO_4, $MgSO_4$, $AlCl_3$, $FeCl_3$, or PEG with different molecular weights (200 Da, 400 Da, 600 Da, 800 Da, 1,000 Da, 1,500 Da, 2,000 Da, 4,000 Da, and 6,000 Da). In particular, both concentrations regarding the salt and PEG solutions were always 2,000 ppm.

The permeate flux (F) was calculated according to the following formula:

$$F = \frac{V}{A \cdot \Delta t} \quad (3)$$

where V, A, and Δt are the volume of the permeation during the test, shell area of the membrane, and the experiment time, respectively.

The solute rejection (R) was calculated according to the following formula:

$$R(\%) = (1 - C_P/C_F) * 100 \quad (4)$$

where C_P and C_F are the permeate concentration and feed concentration, respectively.

The salt concentrations were indirectly measured through the conductivity measured by a conductivity meter (Conductivity-ID944, IT Caster Ltd., China) at room temperature [43]. The concentration of the PEG solution with different molecular weights was measured through a total organic carbon analyzer (TOC-L, Shimadzu, Japan). All samples were analyzed three times and averaged.

The molecular weight cut-off of $\gamma\,\alpha$ HF membrane is defined here as the same as the average molecular weight of PEG with a 90% rejection [44] The mean pore size is defined as the radius of the PEG molecule when the retention rate of the PEG was 90%. Based on average molecular weight, the Stokes diameter of PEG was calculated by the following formula [45]

$$d_n = 0.0262 \times M_p^{0.5} - 0.03 \quad (5)$$

where d_n is the diameter (nm) of the $\gamma\,\alpha$ HF membrane and M_p is the molecular weight (Da) of PEG.

7. Desalination and Concentration

The experiment of removing potassium and sodium ions from lignin wastewater was by the diafiltration method [46]. In this experiment at room temperature, the pump's flow rate was set to 200 ml/min, the operating pressure was 5 bar, and the feed was acidic lignin and alkaline lignin. In the desalination process, assuming that the rejection of the separation membrane to ions is constant, the total permeation amount can be obtained by the material balance equation to achieve the required removal rate [47]. The material balance is obtained as follows:

$$V_0 dC = -CdV \quad (6)$$

Eq. (6) was integrated to get

$$\frac{V_p}{V_0} = -\frac{1}{D}\ln(C_0/C_t) \quad (7)$$

$$D_t = 1 - \frac{C_t}{C_0} = 1 - R \quad (8)$$

So that, combining Eq. (7) and Eq. (8) the ratio between total infiltration volume at the end of the experiment (V_p) and the total volume of feed (V_0) is as follows:

$$\frac{V_p}{V_0} = -\frac{1}{D}\ln(1 - D_t) \quad (9)$$

where D and D_t are the desalination rate of the separation membrane and the final ion removal rate, respectively. Through Eq. (9), when the amount of permeate is 600 ml, the final ion removal rate and the ion rejection are 87.3% and 90%, respectively. Before the experiment, the maximum and minimum level lines in the feed

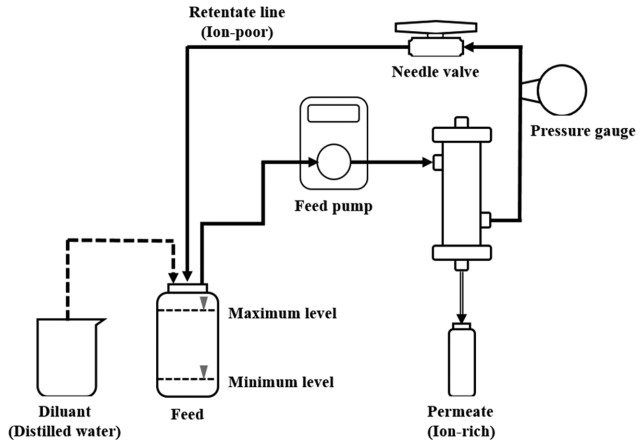

Fig. 1. Experimental process for removal of potassium and sodium ions from lignin wastewater.

tank were marked. In detail, a series of experiments were conducted when the lignin wastewater reached the minimum level of 60 ml. The ion removal experiment was carried out for three cycles. After the first and second cycles, about 200 ml of deionized water was added to the tank to alleviate the concentration and increase the total permeability. The lignin wastewater and retentate were sampled once every 15 min so that the lignin concentration and conductivity were analyzed. After the experiment, the potassium and sodium ions in feed and retentate were analyzed separately to calculate the ion removal rate. The lignin concentration was analyzed by ultraviolet and visible spectrophotometry (UV-vis, Optizen Pop, Mecasys, Korea) at 280 nm [48]. The potassium and sodium ions were analyzed by an inductively coupled plasma optical emission spectrometer (ICP-OES, OPTIMA 8300, PerkinElmer, USA). The calculation formula of ion removal rate (R_a) is as follows:

$$R_a(\%) = \left(1 - \frac{M_r \times C_{ir}}{M_f \times C_{if}}\right) \times 100 \quad (10)$$

where M_r is the mass (g) at retentate, C_{ir} is the ion concentration at retentate, M_f is the mass (g) at feed, and C_{if} is the ion concentration at the feed.

The experimental process is shown in Fig. 1.

8. Long-term Separation Test in Lignin Wastewater

To explore the long-term separation performance of the nanofiltration membrane in lignin wastewater, the long-term operation of the $\gamma\alpha$ HF membrane was carried out within 120 hours, where the rejection of lignin, ions, and the flux was analyzed and recorded. To keep the lignin concentration stable in the wastewater tank, after the analysis the permeate was poured again into the lignin wastewater tank. The experiment was carried out at 25 °C and a pressure of 4 bar. SEM analysis was performed on the $\gamma\alpha$ HF membrane to observe the change of coating structure after the long-term separation test.

RESULTS AND DISCUSSION

1. Characterization of α HF Support and $\gamma\alpha$ HF Membrane

The cross-section and surface SEM images of α HF support and $\gamma\alpha$ HF membrane were provided, as shown in Fig. 2. By comparing the surface images of α HF support (Fig. 2(c)) and $\gamma\alpha$ HF membrane (Fig. 2(d)), it can be seen that the α HF support has a rough surface layer with large voids, while the $\gamma\alpha$ HF membrane has a surface layer without any observable defects. In addition, it can be seen from the section image that the $\gamma\alpha$ HF membrane has a finger-like pore structure. From Fig. 2(a), (b), (e), and (f), there was a uniform and dense γ-Al_2O_3 coating layer on the surface of the porous α HF support. Finally, it can be seen from the enlarged section images (see Fig. 2(g) and Fig. 2(h)) that the thickness of the γ-Al_2O_3 coating layer was about 4 μm.

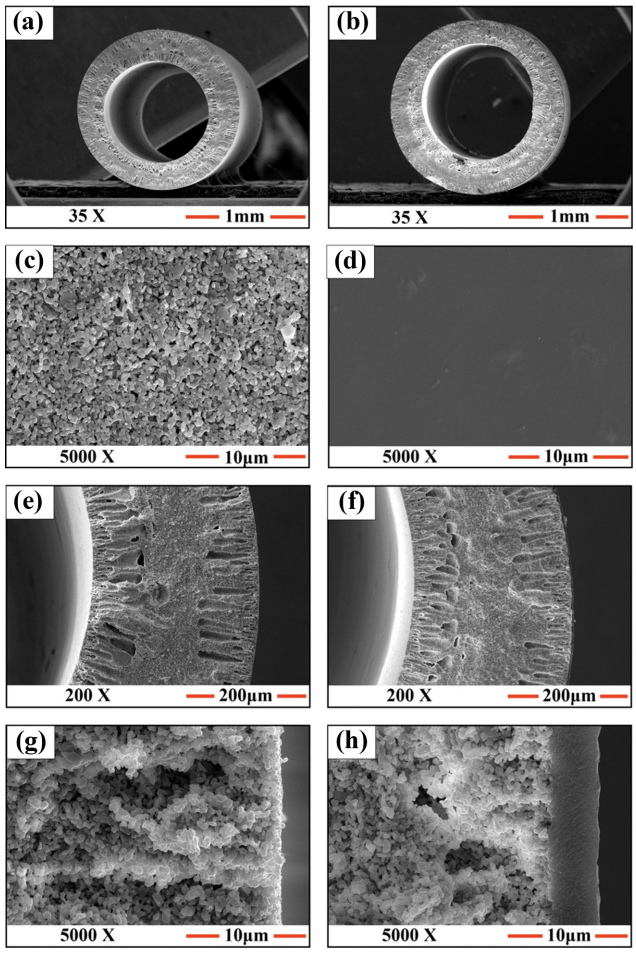

Fig. 2. SEM images of (a), (c), (e), (g) α HF support and (b), (d), (f), (h) $\gamma\alpha$ HF membrane.

The water contact angle images of α HF support and $\gamma\alpha$ HF membrane are shown in Fig. 3(a) and Fig. 3(b), respectively. From Fig. 3(a) the average water contact angle of the α HF support was about 25.42°. After the deposition of a dense γ-Al_2O_3 coating layer, the average water contact angle of the $\gamma\alpha$ HF membrane was 57.9°. Therefore, it can be concluded that the α HF support had higher hydrophilicity than that of the $\gamma\alpha$ HF membrane. The reason behind this behavior is that the low hydrophilicity characteristics of the $\gamma\alpha$ HF membrane may be due to the small pore size relative to the α HF support.

The porosity of α HF support and the $\gamma\alpha$ HF membrane was

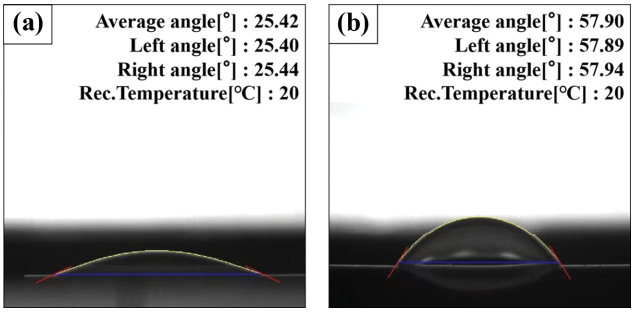

Fig. 3. Dynamic contact angles of (a) α HF support and (b) $\gamma\alpha$ HF membrane.

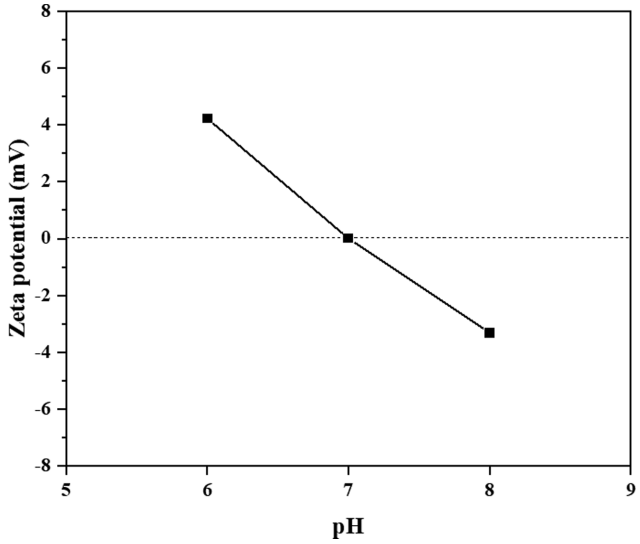

Fig. 4. Zeta potential of γ-Al_2O_3 powder in different pH conditions.

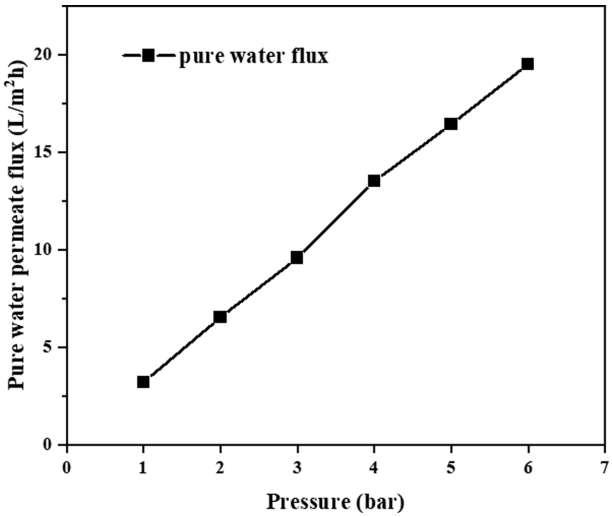

Fig. 5. Water permeate flux for the $\gamma\alpha$ HF membrane under different pressure conditions.

Table 1. Various salts rejection of $\gamma\alpha$ HF membrane

Salt	Mean rejection/%	Standard D
Na_2SO_4	7.53	0.15
$MgSO_4$	8.89	0.46
NaCl	15.30	0.50
KCl	15.71	0.23
$CaCl_2$	67.01	2.42
$MgCl_2$	72.65	2.43
$AlCl_3$	86.82	2.22

calculated by Eq. (2). The porosity of the α HF support and $\gamma\alpha$ HF membrane was 54.3% and 46.4%, respectively. It also proved that the hydrophilicity of the γ-Al_2O_3/α-Al_2O_3 nano-filtration membrane was slightly lower than that of the support. The decrease in hydrophilicity of the nano-filtration membrane was mainly caused by the decrease in the membrane's pore size [49].

Fig. 4 shows the measurement results of the zeta potential analysis of the γ-Al_2O_3 colloidal suspension. The γ-Al_2O_3 powder surface shows a positive charge when the solution was acidic for HCl and a negative charge when the solution was basic for NaOH. In addition, the point of zero charge was found equal to 7. It can therefore be conjectured that when the membrane is operated under acidic conditions, the separation characteristics for monovalent cations are mainly derived from the pore size of the separation membrane. In contrast, when the membrane is operated under alkaline conditions, the separation characteristics are a combination of pore size and surface charge. This means that the Donnan effect is better under acidic conditions than under acidic conditions.

2. Permeation Test and Main Pore Size

The pure water permeate flux for the $\gamma\alpha$ HF membrane is shown in Fig. 5, where it can be seen that the pure water permeate flux was 3.45 L/m^{2}h with a pure water flux and under the pressure of 1 bar. In addition, there is a positive correlation between pure water permeate flux (L/m^{2}h) and pressure (bar). In fact, the pure water permeate fluxes increased with increasing the pressure to a maximum of 20 L/m^{2}h for a pressure of 6 bar.

Table 1 shows the results of various salt rejection (%) of $\gamma\alpha$ HF membrane. According to these results, the rejection of monovalent cations is significantly lower than that of polyvalent cations and then, in turn, $\gamma\alpha$ HF membrane shows the characteristics of distinguishing monovalent from polyvalent ions. Also, the rejection of Na_2SO_4 was lower than that of NaCl, and the rejection of $MgSO_4$ was lower than $MgCl_2$ because the prepared $\gamma\alpha$ HF membrane was positively charged and SO_4^{2-} was divalent, in good agreement with previous studies [50]. Therefore, the $\gamma\alpha$ HF membrane had the property of separating multivalent and monovalent ions during operation. The different rejections shown in Table 1 were related to the hydration radius of ions. Table 2 shows some properties of related cations studied in this work so that it can be concluded that the rejection property of the $\gamma\alpha$ HF membrane is related to the hydration radius of ions. However, the rejection of monovalent and divalent ions was quite different, and the rejection of cut SO_4^{2-} was significantly lower than that of Cl^-, indicating that the Donnan effect on the $\gamma\alpha$ HF membrane was greater than that of membrane pore size.

Fig. 6 shows the rejection of PEG with different molecular weights.

Table 2. Properties of related cations [51]

Element	Ion weight/ Da	Ionic radius/ nm	Hydrated radius/ nm
Na^+	23.0	0.095	0.358
K^+	39.0	0.133	0.331
Ca^{2+}	40.0	0.113	0.412
Mg^{2+}	24.3	0.065	0.428
Al^{3+}	27.0	0.050	0.475
Cl^-	35.5	0.181	0.332
SO_4^{2-}	96.0	0.245	0.300

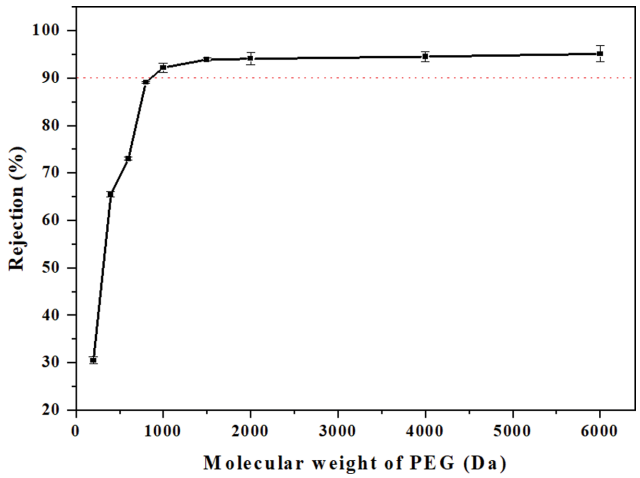

Fig. 6. PEG retention of $\gamma\alpha$ HF membrane.

It can be seen from Fig. 7 that the $\gamma\alpha$ HF membrane has more than 90% rejection of PEG above 1,000 Da, so the molecular weight cut-off of the $\gamma\alpha$ HF membrane is 1,000 Da. Because the molecular weight of lignin is mostly distributed between 1,020 Da and 60,000 Da [52-55], the $\gamma\alpha$ HF membrane can be used for ion removal from lignin wastewater and lignin concentration.

The mean pore sizes of the α HF support and the $\gamma\alpha$ HF membrane were determined according to Eqs. (1) and (2) and found to be 0.2 μm and 1.6 nm, respectively.

3. Desalination and Concentration of Lignin Wastewater

Fig. 7 shows the photographs of the permeate, feed and retentate solutions. It can be seen from Fig. 7(a) that the color of the liquid flowing out from the permeate end of the $\gamma\alpha$ NF membrane is clear and transparent. The retentate solution (see Fig. 7(c)) is not only darker than that of the feed solution (see Fig. 7(b)), but

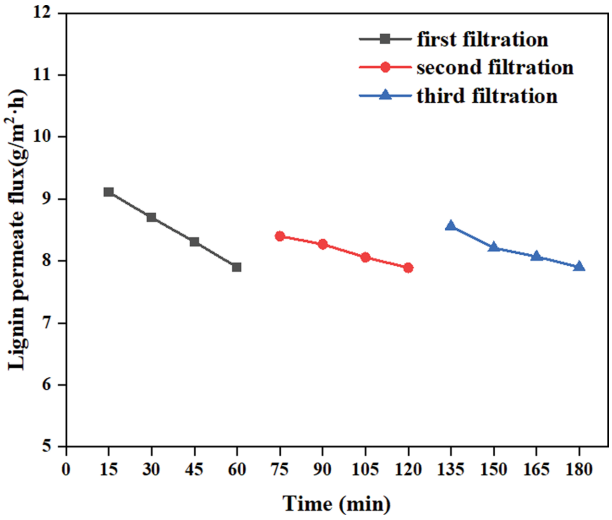

Fig. 8. Lignin permeate flux versus operating time during three successive experimental cycles of desalination and concentration process for the $\gamma\alpha$ HF membrane.

also the tangential transparency of the retentate solution (see Fig. 7(c)) is lower than that feed solution (see Fig. 7(b)). This observation can be rationalized by considering that lignin in lignin wastewater was concentrated.

Fig. 8 shows the lignin permeate flux during three successive experimental cycles. At the beginning of the experiment, the lignin permeate flux obtained with a $\gamma\alpha$ HF membrane was about 9.2 g/m^{2}hr. After the first and second water additions, the lignin permeate fluxes were in the range of about 8.7-8.6 g/m^{2}hr, respectively. From these results, it can be seen that the decrease of the lignin permeate flux at the beginning of the experiments was caused by deterioration of the pores. The reason for the decrease of flux after each water addition is that the concentration in the lignin wastewater tank will become thicker with the operation time.

It can be seen from Fig. 9 that the conductivity of the lignin wastewater tank decreases with increasing the operation time and water addition. An explanation of these results could be that with the increased running time, the water in the wastewater gradually passes through the $\gamma\alpha$ HF membrane, resulting in little difference in ion concentration in the wastewater tank. With the discharge of ions, the change of conductivity of the retentate solution was gradually reduced after each cycle. The $\gamma\alpha$ HF membrane can achieve efficient removal performance, but it cannot reach a 100% removal rate. In each nano-filtration process through $\gamma\alpha$ HF membrane, the conductivity of retentate solution decreases with the increase

Fig. 7. Solution of (a) permeate, (b) feed, and (c) retentate.

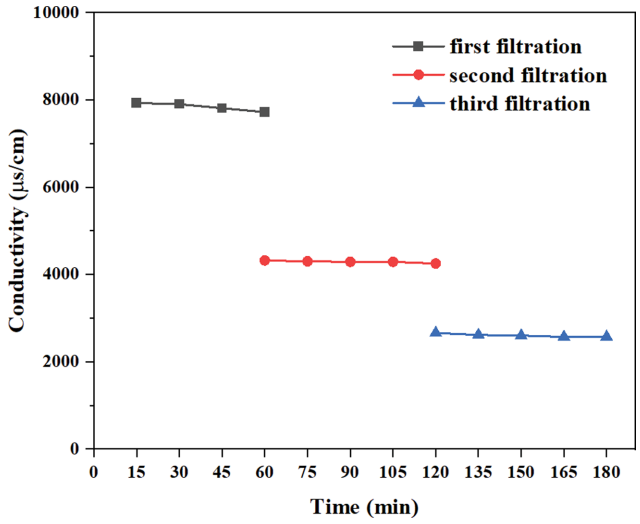

Fig. 9. The conductivity of retentate solution with operating time in the desalination process for the $\gamma\alpha$ HF membrane.

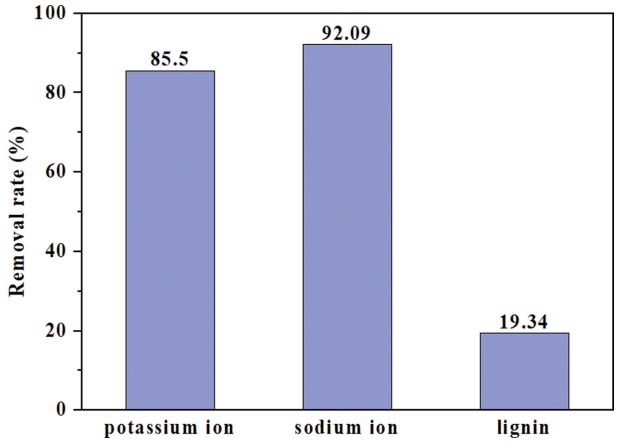

Fig. 10. The removal rate of potassium, sodium ions, and lignin after 180 min of desalination process through the $\gamma\alpha$ HF membrane.

of ions removal amount, but the effect of complete removal cannot be achieved.

Potassium and sodium ion concentrations were estimated by the ICP-OES analysis. The results of UV-Vis analysis on the concentration of lignin were calculated by Eq. (10). Fig. 10 shows the removal rate of potassium, sodium ions, and lignin after 180 min of desalination process through the $\gamma\alpha$ HF membrane. It can be seen that the removal rate of sodium ions reached 92.09%, as well as the removal rate of potassium ions reached about 85.5%, which proves that the $\gamma\alpha$ HF membrane can effectively remove sodium and potassium ions from the lignin wastewater. However, while potassium and sodium ions were removed, 19.34% of lignin was still removed through the membrane because of the non-uniform pore size distribution of the prepared $\gamma\alpha$ HF membrane. This amount of lignin may be caused by the small part of molecular weight passing through the large pore size of the $\gamma\alpha$ HF membrane, and the removal rate was 19.34% was similar to the removal

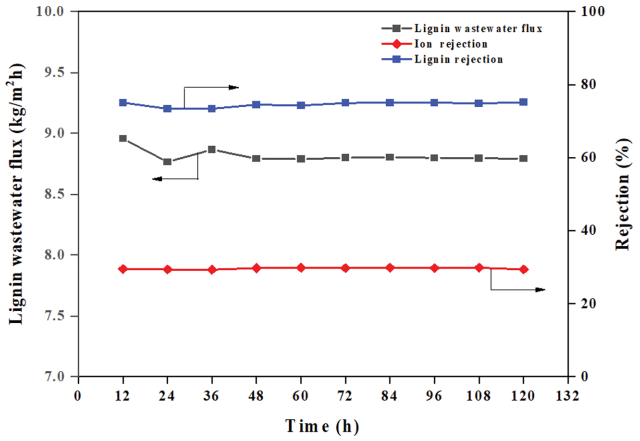

Fig. 11. The flux of lignin wastewater, ion rejection rate, and lignin rejection rate in a five day long experiment.

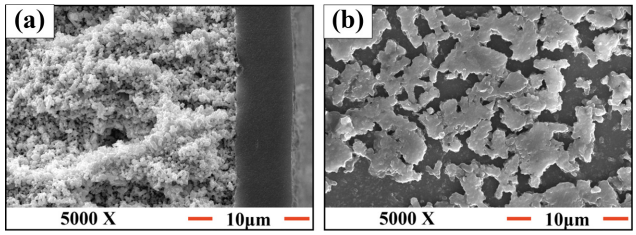

Fig. 12. SEM images of the (a) cross-section and (b) the surface of the $\gamma\alpha$ HF membrane after a long-term experiment (five days).

rate calculated by Eq. (9), which proves that Eq. (9) is also suitable to calculate the removal rate of potassium and sodium ions in lignin wastewater.

4. Long-term Test

The flux, lignin rejection, and ion rejection of the $\gamma\alpha$ HF membrane in lignin wastewater were recorded continuously during a five day long experiment (see Fig. 11). It can be seen that the lignin wastewater flux changed in the first 24 hours, which may be due to the membrane surface. The average lignin wastewater flux was independent of time after 24 hours, so the influence of running time on the lignin wastewater flux and then on the performance of the $\gamma\alpha$ HF membrane was irrelevant. As can be noted in Fig. 11, the ion rejection rate was found to be independent of the time at about 29% during the five day long-term experiment. The lignin rejection rate has a weakly increasing trend with time. In detail, with the increase of time, some white patches formed on the surface of the membrane with the result of an increase of lignin rejection rate with time.

According to Fig. 12, effectively there is a thin film formed by wastewater on the surface of the $\gamma\alpha$ HF membrane and, in turn, surface contamination accompanied by a decrease in pore size. In addition, there was no crack and hole on the surface of the $\gamma\alpha$ HF membrane, indicating that the five day long experiment did not cause any structural damage to the $\gamma\alpha$ HF membrane. From the cross-section SEM image of the $\gamma\alpha$ HF membrane, the thickness of the dense γ-Al_2O_3 coating layer did not increase significantly, and it existed continuously on the α HF support. In conclusion,

the proposed $\gamma\alpha$ HF membrane shows not only a high removal efficiency but also has stable performance under a long time operation (five days).

CONCLUSIONS

A nano-filtration hollow fiber membrane with a mean pore diameter of 1.64 nm and molecular retention of 1,000 Da was successfully prepared. The γ-Al_2O_3 film-coated porous α-Al_2O_3 hollow fiber ($\gamma\alpha$ HF) membrane had a pure water flux of 3.3 L/m^{2}h at a pressure of 1 bar. In a single salt solution, a filtration experiment can have a 15% rejection of monovalent ions and a higher rejection of divalent ions. Moreover, the effect of diafiltration on nano-filtration in wastewater was verified, and diafiltration could reasonably deal with the application of nano-filtration membrane in wastewater.

The prepared $\gamma\alpha$ HF membrane can be removed about 93% and 85% of sodium and potassium ions in lignin wastewater, respectively, but about 19% of the lignin was released as filtration proceeded. Moreover, the clear solution at the permeate end can also be recycled as it is rich in potassium and sodium ions.

The flux of lignin wastewater, ion rejection rate, and lignin rejection remains essentially unchanged for a long time (five days) one-step nano-filtration process for lignin desalination and concentration. In conclusion, the superior desalination and lignin concentration properties in a lignin aqueous solution, in particular, make $\gamma\alpha$ HF membrane attractive for use in nano-filtration processes.

ACKNOWLEDGEMENTS

This work was supported by the framework of the research-development program of the Korean Institute of Energy Research (C0-2427-01), Republic of Korea.

REFERENCES

1. Y. L. Ji, W. J. Qian, Y. W. Yu, Q. F. An, L. F Liu, Y. Zhou and C. J. Gao, *Chin. J. Chem. Eng.*, **25**, 11 (2017).
2. J. A. Poveda-Giraldo, J. C. Solarte-Toro and C. A. C. Alzate, *Renew. Sust. Energ. Rev.*, **138**, 110688 (2021).
3. J. H. Park, M. H. Jin, Y. J. Lee, G. S. Song, J. W. Choi, D. W. Lee, Y. C. Choi, S. J. Park, K. H. Song and J. G. Kim, *Energies*, **12**, 16 (2019).
4. L. Cao, I. K. M. Yu, Y. Liu, X. Ruan, D. C. W. Tsang, A. J. Hunt, Y. S. Ok, H. Song and S. Zhang, *Bioresour. Technol.*, **269**, 465 (2018).
5. E. Ahmad and K. K. Pant, Waste Biorefinery Potential and Perspectives, 409 (2018).
6. B. M. Upton and A. M. Kasko, *Chem. Rev.*, **116**, 4 (2016).
7. A. W. Mohammad, Y. H. Teow, W. L. Ang, Y. T. Chung, D. L. Oatley-Radcliffe and N. Hilal, *Desalination*, **356**, 226 (2015).
8. C. Liu, Y. Jiang, A. Nalaparaju, J. Jiang and A. Huang, *J. Mater. Chem. A*, **7**, 24205 (2019).
9. M. B. M. Y. Ang, C. L. Tang, M. R. D. Guzman, H. L. C. Maganto, A. R. Caparanga, S. H. Huang, H. A. Tsai, C. C. Hu, K. R. Lee and J. Y. Lai, *Desalination*, **481**, 114352 (2020).
10. H. Niemi, J. Lahti, H. Hatakka, S. Kärki, S. Rovio, M. Kallioinen, M. Mänttäri and M. Louhi-Kultanen, *Chem. Eng. Technol.*, **34**(4), 593 (2011).
11. M. Liu, G. Yao, Q. Cheng, M. Ma, S. Yu and C. Gao, *J. Membr. Sci.*, **415-416**, 122 (2012).
12. M. Dalwani, G. Bargeman, S. S. Hosseiny, M. Boerrigter, M. Wessling and N. E. Benes, *J. Membr. Sci.*, **381**(1-2), 81 (2011).
13. S. De and P. K. Bhattacharya, *J. Membr. Sci.*, **109**(1), 109 (1996).
14. C. Pateraki, D. Ladakis, L. Stragier, W. Verstraete, I. Kookos, P. Seraphim and A. Koutinas, *J. Biotechnol.*, **233**, 95 (2016).
15. P. K. Bhattacharya, R. K. Todi, M. Tiwari, C. Bhattacharjee, S. Bhattacharjee and S. Datta, *Desalination*, **174**(3), 287 (2005).
16. O. Ringena, B. Saake and R. Lehnen, *Wood Sci. Technol.*, **59**(4), 405 (2005).
17. M. Olivares, J. A. Guzmán, A. Natho and A. Saavedra, *Wood Sci. Technol.*, **22**, 157 (1988).
18. S. Bhattacharjee, S. Datta and C. Bhattacharjee, *J. Clean Prod.*, **14**(5), 497 (2006).
19. S. Satyanarayana, P. Bhattacharya and S. De, *Sep. Purif. Technol.*, **20**(2-3), 155 (2000).
20. O. Wallberg, A. Jönsson and R. Wimmerstedt, *Desalination*, **154**(2), 187 (2003).
21. M. Ebrahimi, S. Kerker, S. Daume, M. Geile, F. Ehlen, I. Unger, S. Schütz and P. Czermak, *Desalin. Water Treat.*, **55**(13), 3554 (2015).
22. O. Wallberg, A. Jönsson and R. Wimmerstedt, *Desalination*, **156**(1-3), 145 (2003).
23. A. Keyoumu, R. Sjödahl, G. Henriksson, M. Ek, G. Gellerstedt and M. E. Lindström, *Ind. Crops Prod.*, **20**(2), 143 (2004).
24. A. Holmqvist, O. Wallberg and A. Jönsson, *Chem. Eng. Res. Des.*, **83**(8), 994 (2005).
25. A. Dafinov, J. Font and R. Garcia-Valls, *Desalination*, **173**(1), 83 (2005).
26. O. Wallberg and A. Jönsson, *Desalination*, **195**(1-3), 187 (2006).
27. A. Jönsson, A. Nordin and O. Wallberg, *Chem. Eng. Res. Des.*, **86**(11), 1271 (2008).
28. A. Toledano, L. Serrano, A. Garcia, I. Mondragon and J. Labidi, *Chem. Eng. J.*, **157**(1), 93 (2010).
29. A. Arkell, J. Olsson and O. Wallberg, *Chem. Eng. Res. Des.*, **92**(9), 1792 (2014).
30. M. Ebrahimi, N. Busse, S. Kerker, O. Schmitz, M. Hilpert and P. Czermak, *Membranes*, **6**(1), 7 (2016).
31. N. Giummarella, C. Lindgren, M. Lindström and G. Henriksso, *BioResources*, **11**(2), 3494 (2016).
32. A. Larbot, S. Alami-Younssi, M. Persin, J. Sarrazin and L. Cot, *J. Membr. Sci.*, **97**, 167 (1994).
33. P. Puhlfürß, A. Voigt, R. Weber and M. Morbé, *J. Membr. Sci.*, **174**(1), 123 (2000).
34. T. V. Gestel, C. Vandecasteele, A. Buekenhoudt, C. Dotremont, J. Luyten, R. Leysen, B. V. Bruggen and G. Maes, *J. Membr. Sci.*, **207**(1), 73 (2002).
35. Z. Sadeghian, F, Zamani and S. N. Ashrafizadeh, *Desalin. Water Treat.*, **20**(1-3), 80 (2010).
36. H. Qi, S. Niu, X. Jiang and N. Xu, *Ceram. Int.*, **39**(3), 2463 (2013).
37. X. Chen, W. Zhang, Y. Lin, Y. Cai, M. Qiu and Y. Fan, *Micropor. Mesopor. Mater.*, **214**, 195 (2015).
38. E. Magnone, M. K. Kim, H. J. Lee and J. H. Park, *Ceram. Int.*, **45**(3), 3359 (2019).
39. E. Magnone, H. J. Lee, J. W. Che and J. H. Park, *J. Ind. Eng. Chem.*,

42, 19 (2016).
40. X. Zhuang, M. C. Shin, B. J. Jeong, S. H. Lee and J. H. Park, *Korean Chem. Eng. Res.*, **59**(2), 174 (2021).
41. K. Li, J. F. Kong, D. Wang and W. K. Teo, *AIChE*, **45**(6), 1211 (1999).
42. Z. Wang, Y. M. Wei, Z. L. Xu, Y. Cao, Z. Q. Dong and X. L. Shi, *J. Membr. Sci.*, **503**, 69 (2016).
43. F. Prieto, E. Barrado, M. Vega and L. Deban, *Russ. J. Appl. Chem.*, **74**, 1321 (2001).
44. Y. Liu, J. Wang, Y. Wang, H. Zhu, X. Xu, T. Liu and Y. Hu, *Chem. Eng. J.*, **405**, 127051 (2021).
45. H. Guo, S. Zhao, X. Wu and H. Qi, *Micropor. Mesopor. Mater.*, **260**, 125 (2018).
46. A. Servent, F. A. P. Abreu, C. Dhuique-Mayer, M. Belleville and M. Dornier, *Innov. Food Sci. Emerg. Technol.*, **66**, 102519 (2020).
47. J. Luo, L. Ding, X. Chen and Y. Wan, *Sep. Purif. Technol.*, **66**(3), 429 (2009).
48. D. Fengel, G. Wegener and J. Feckl, *Holzforschung*, **35**(3), 111 (1981).
49. F. Xu, M. Wei, X. Zhang, Y. Song, W. Zhou and Y. Wang, *Research*, **2019**, 2581241 (2019).
50. Z. Wang, Y. Wei, Z. Xu, Y. Cao, Z. Dong and X. Shi, *J. Membr. Sci.*, **503**, 69 (2016).
51. B. Tansel, *Sep. Purif. Technol.*, **86**, 119 (2012).
52. A. Tolbert, H. Akinosho, R. Khunsupat, A. K. Naskar and A. J. Ragauskas, *Biofuels Bioprod. Biorefining*, **8**(6), 836 (2014).
53. W. G. Glasser, V. Davé and C. E. Frazier, *J. Wood Chem. Technol.*, **13**(4), 545 (1993).
54. W. Brown, *J. Appl. Polym. Sci.*, **11**(11), 2381 (1967).
55. D. Dong and A. L. Fricke, *Polymer*, **36**(10), 2075 (1995).